5th International Symposium on Hydraulic Structures
Hydraulic Structures and Society: Engineering Challenges and Extremes
ISBN 9781742721156 - DOI: 10.14264/uql.2014.34
Brisbane, Australia, 25-27 June 2014

Pressure Fluctuations and Air-Water Flow Properties in Hydraulic Jumps

H. Wang[1], F. Murzyn[2] and H. Chanson[1]
[1]The University of Queensland, School of Civil Engineering
Brisbane QLD 4072
AUSTRALIA
E-mail: h.chanson@uq.edu.au
[2]ESTACA Campus Ouest, Parc Universitaire de Laval Changé
Rue Georges Charpak, BP 76121, 53061 Laval Cedex 9
FRANCE

Abstract: *A hydraulic jump is a rapidly-varied flow associated by large and rapid fluctuations of its two-phase properties. Herein a miniature total pressure probe was used simultaneously with a phase-detection probe and several acoustic displacement meters to characterise the instantaneous air-water turbulent properties and the free surface fluctuations. New laboratory experiments were performed for a range of Froude numbers ($3.8 < Fr_1 < 8.5$). The total pressure was measured within the turbulent shear region showing maximum mean pressure and maximum pressure fluctuations slightly above the invert. The interactions between the instantaneous total pressure, void fraction and free-surface fluctuations were detailed based upon some correlation analyses. Altogether the experimental method provided a greater level of details into the instantaneous two-phase flow properties, highlighting the large and rapid fluctuations of the two-phase flow properties at the millimetric and sub-millimetric scales.*

Keywords: *Hydraulic jumps, Total pressure probe, Pressure fluctuations, Air-water properties, Instrumentation, Physical modelling*

1. INTRODUCTION

A hydraulic jump is a rapidly-varied open channel flow characterised by the sudden transition from a supercritical flow motion to a subcritical regime. The transition is associated with a rapid increase of water depth, a highly turbulent flow with macro-scale vortices, significant kinetic energy dissipation, a two-phase flow region and some strong turbulence interactions with the free surface leading to splashes and droplet formation (Fig. 1). Industrial applications include energy dissipators downstream of high-velocity spillways, in-stream re-aeration structures, and mixing enhancement (Avery and Novak 1978, Hager 1992). Leisurely applications encompass artificial generation of hydraulic jumps in river streams and man-made course for extreme sports such as kayaking and rafting.

The application of the continuity and momentum principles yields a relationship between the upstream and downstream cross-section areas and the inflow Froude number Fr_1 (Chanson 2012). For a hydraulic jump in an irregular prismatic channel, it gives:

$$\frac{A_2}{A_1} = \frac{1}{2} \times \frac{\sqrt{\left(2 - \frac{B'}{B}\right)^2 + 8 \times \frac{\frac{B'}{B}}{\frac{B_1}{B}} \times Fr_1^2} - \left(2 - \frac{B'}{B}\right)}{\frac{B'}{B}} \quad (1)$$

where A is the flow cross-section area, the subscripts 1 and 2 refer to the upstream and downstream properties respectively, B_1 is the upstream free-surface width, Fr_1 is the inflow Froude number, and B and B' are characteristic channel widths defined respectively as:

$$Fr_1 = \frac{V_1}{\sqrt{g \times \frac{A_1}{B_1}}} \quad (2)$$

$$B = \frac{A_2 - A_1}{d_2 - d_1} \quad (3)$$

$$B' = \int_{A_1}^{A_2} \int \rho \times g \times (d_2 - y) \times dA \Big/ \left(\frac{1}{2} \times \rho \times g \times (d_2 - d_1)^2 \right) \quad (4)$$

with V_1 and d_1 being the inflow velocity and depth respectively and g the gravity acceleration. For a rectangular channel, B = B' = B_1, and $Fr_1 = V_1/(g \times d_1)^{1/2}$.

In this study, a miniature total pressure probe was used to record simultaneously the instantaneous flow properties together with a phase-detection probe and five acoustic displacement meters. It is the aim of this study to characterise in details the instantaneous two-phase turbulent flow in hydraulic jumps. The metrology was applied to new laboratory experiments conducted for a range of Froude number ($3.8 < Fr_1 < 8.5$).

Figure 1 – Experimental hydraulic jump - Flow conditions: Q = 0.0399 m^3/s, d_1 = 0.020 m, x_1 = 0.83 m, Fr_1 = 8.5, Re = 7.9×10^4 - Flow direction from left to right

2. PHYSICAL MODELLING AND INSTRUMENTATION

Any theoretical and numerical analyses of hydraulic jumps are based upon a large number of relevant equations to describe the two-phase turbulent flow motion and the interactions between entrained air and turbulence. The outputs must be tested against a broad range of gas-liquid flow measurements: "*Unequivocally [...] no experimental data means no validation*" (Roache 2009). Physical modelling requires the selection of a suitable dynamic similarity (Liggett 1994, Chanson 2013). Considering a hydraulic jump in a smooth horizontal rectangular channel, dimensional considerations give a series of dimensionless relationships in terms of the turbulent two-phase flow properties at a position (x,y,z) within the hydraulic jump roller as functions of the inflow properties, fluid properties and channel configurations. Using the upstream flow depth d_1 as the characteristic length scale, a dimensional analysis yields:

$$\frac{P}{0.5 \times \rho \times V_1^2}, \frac{p'}{0.5 \times \rho \times V_1^2}, \frac{V}{V_1}, \frac{v'}{V_1}, C, \frac{F \times d_1}{V_1}, ... = F\left(\frac{x - x_1}{d_1}, \frac{y}{d_1}, \frac{z}{d_1}, Fr_1, Re, \frac{v_1'}{V_1}, \frac{x_1}{d_1}, \frac{W}{d_1}, ... \right) \quad (5)$$

where P and V are the pressure and velocity respectively, p' and v' are pressure and velocity fluctuations, C is the void fraction, F is the bubble count rate, x_1 is the jump toe position, Re is the Reynolds number, W is the channel width and the subscript 1 refers to the inflow conditions. In a hydraulic jump, the momentum considerations demonstrated the significance of the inflow Froude number (see above) and the selection of the Froude similitude derives implicitly from basic theoretical

considerations (Liggett 1994, Chanson 2012). Equation (5) shows that measurements in small size models might be affected by viscous scale effects because the Reynolds number is grossly underestimated. In the present study, the experiments were performed in a relatively large-size facility to minimise scale effects following Murzyn and Chanson (2008).

New experiments were performed in a horizontal rectangular flume (Fig. 1). The channel was 0.5 m wide and 3.2 m long, the sidewalls were made of glass while the bed was made out of very smooth HDPE. The inflow was controlled by an upstream rounded undershoot gate and the downstream flow conditions were controlled by a vertical overshoot gate. Herein the inflow depth was d_1 = 0.020 m, the distance between jump toe and upstream gate was x_1 = 0.83 m, and the inflow Froude number ranged from 3.8 to 8.5, corresponding to Reynolds numbers between 3.5×10^4 and 8×10^4. The instantaneous flow properties were measured using a total pressure probe, a phase-detection probe and a series of acoustic displacement meters sampled simultaneously at 5 kHz for 180 s.

The total pressure probe consisted of a silicon diaphragm sensor mounted on a probe (Fig. 2). The sensor was a miniature pressure transducer manufactured by MeasureX (Model MRV21). The sensitive part had a 5 mm outer diameter. A signal amplification system filtered the signal to eliminate noises above 2 kHz. During the experiments, the sensor was mounted close to the phase-detection probe: the transversal distance between both was adjusted to 9 mm. A daily calibration was conducted and regularly checked, because the output voltage appeared to be temperature sensitive. Note that such a diaphragm pressure sensor is not affected by the presence of bubbles and does not require to be purged. The dual-tip phase-detection probe was manufactured based upon a needle design to pierce bubbles and droplets and worked based upon the difference in electrical resistance between air and water. The probe was equipped with two identical needle sensors with an inner diameter of 0.25 mm. The longitudinal distance between probe tips was 7.25 mm (Fig. 2). The phase-detection probe was excited by an electronic system (Ref. UQ82.518) designed with a response time of less than 10 µs. The vertical elevation of the probes was controlled by a Mitutomo™ digimatic scale unit with an accuracy of 0.01 mm. The instantaneous free-surface elevation above the phase-detection leading tip was recorded non-intrusively using a Microsonic™ Mic+25/IU/TC acoustic displacement meter, and further Microsonic™ Mic+25/IU/TC acoustic displacement meters were located above the roller free-surface. The measurement range was from 30 to 250 mm with 0.18 mm accuracy and 50 ms response time.

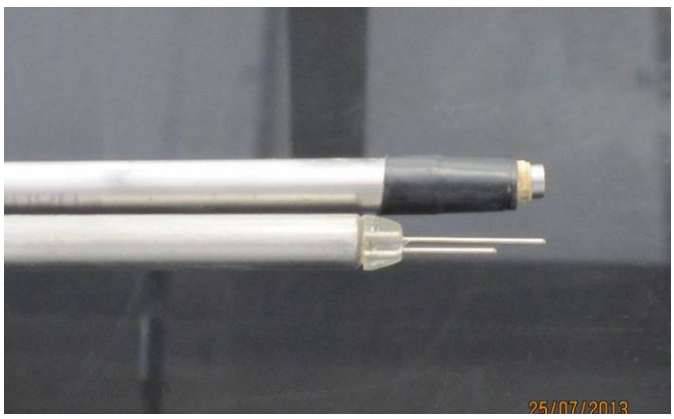

Figure 2 – Pressure probe mounted beside the dual-tip phase-detection probe (view in elevation) with a flow direction from right to left.

3. BASIC FLOW PATTERNS

The measurements of instantaneous water elevation η at several longitudinal positions outlined the mean free surface profile and its fluctuations. Some typical results are shown in Figure 3A and 3B respectively. The time-averaged free surface profiles were comparable to photographic observations through the glass sidewall (Fig. 1). The downstream conjugate depth and jump roller length increased with increasing Froude number. The ratio of conjugate depths followed closely Equation (1). The jump roller length L_r was defined as the distance over which the water depth increases monotonically. The data were close to earlier observations and they followed closely an empirical correlation:

$$\frac{L_r}{d_1} = 5.8 \times (Fr_1 - 0.9) \quad (6)$$

Within the roller length, the time-averaged free-surface profiles presented a self-similar shape (Fig. 3B) which was best fitted by:

$$\frac{\eta - d_1}{d_2 - d_1} = \left(\frac{x - x_1}{L_r}\right)^{0.56} \qquad 0 < (x-x_1)/L_r < 1 \quad (7)$$

The instantaneous deformations of the free-surface were large and rapid above the roller. The free-surface fluctuation magnitude increased with the inflow Froude number. The maximum fluctuations were seen close to and downstream of the jump toe (Fig. 3C). The characteristic frequency of the free-surface fluctuation was found in a range of 1.7 to 3.7 Hz. It was shown slightly higher for small Froude numbers as well as in the first half roller than that further downstream.

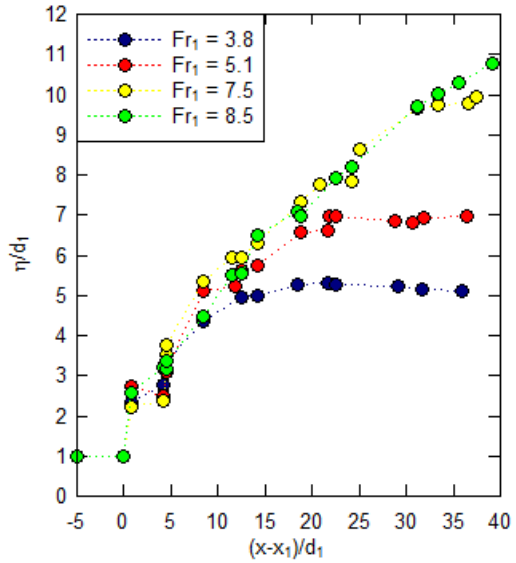

(A, Left) Time-averaged free-surface profiles

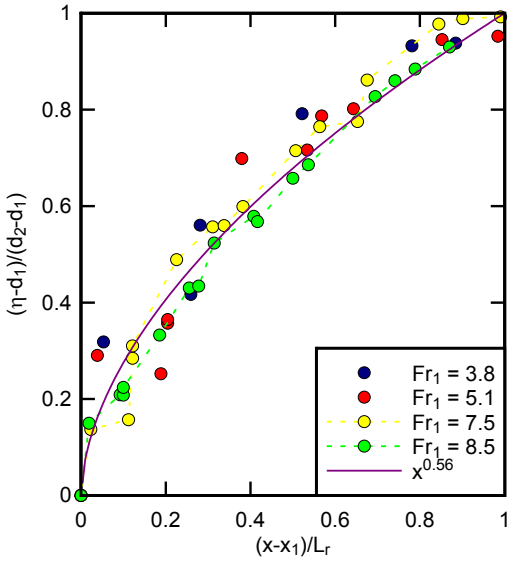

(B, Right) Self-similar roller surface profiles

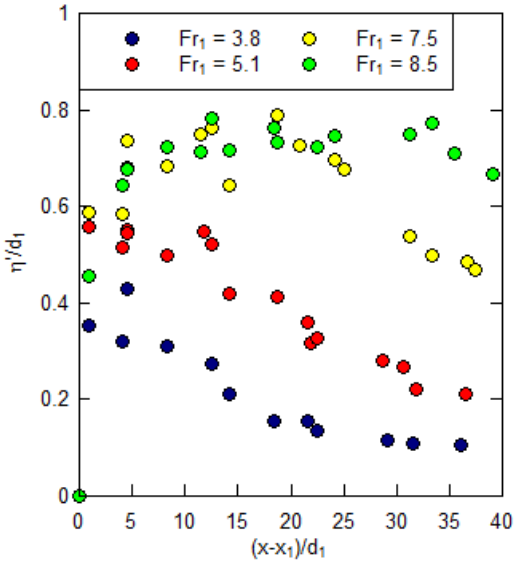

(C) Standard deviations of water elevations

Figure 3 – Free-surface profiles and free-surface fluctuations of hydraulic jumps.

4. TOTAL PRESSURE AND AIR-WATER PROPERTIES

The air-water flow properties were measured at several cross sections in the jump roller. The results in terms of the time-averaged void fraction, bubble count rate and interfacial velocity distributions showed two characteristic air-water flow regions, namely a turbulent shear region and a recirculation region above (Fig. 4). Figure 4 illustrates some typical air-water flow data measured with the dual-tip phase-detection probe in a hydraulic jump (Fr_1 = 7.5), where η is the mean water elevation measured with the acoustic displacement meters and y_* is the elevation of a local minimum in void fraction. In the lower shear region, the entrapped air was advected downstream, and the void fraction distribution followed a bubble diffusion solution (Chanson 1995,2010). The interfacial velocity distributions showed a shape close to a wall jet solution, with a maximum velocity close to the bottom and a region where the velocity decreased with increasing elevation above. In the upper recirculation region next to the free surface, the void fraction increased rapidly with increasing vertical elevation, while the mean flow direction was negative.

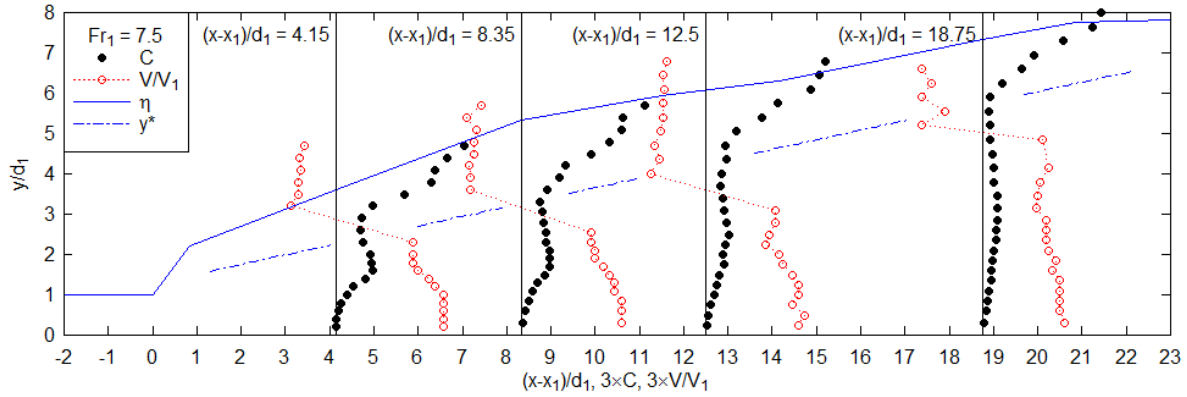

Figure 4 – Vertical distributions of time-averaged void fraction and interfacial velocity in a hydraulic jump – Flow conditions: Q = 0.0347 m^3/s, d_1 = 0.020 m, x_1 = 0.83 m, Fr_1 = 7.5, Re = 6.8×10^4.

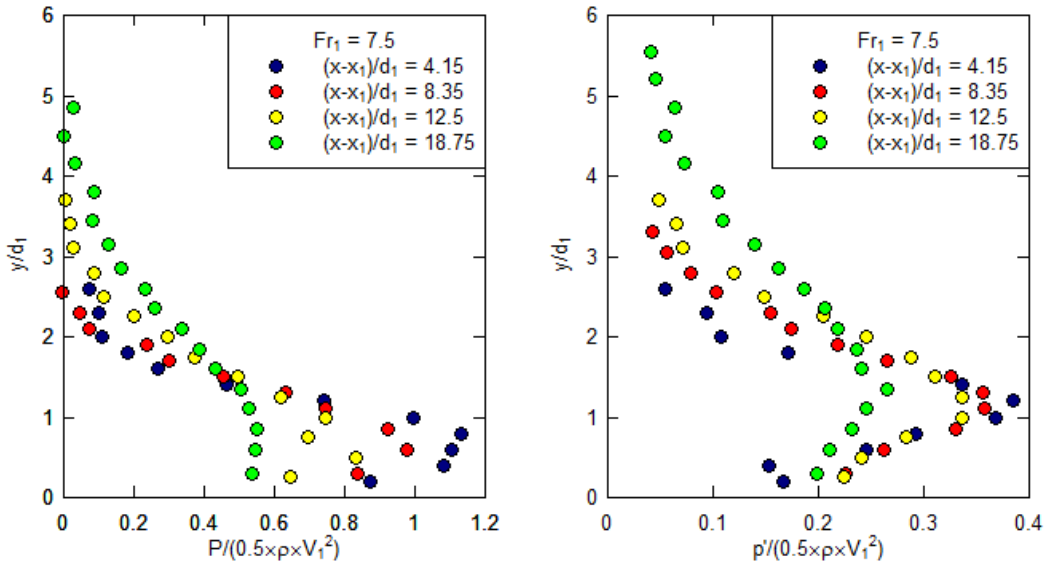

(A, Left) Time-averaged total pressure (B, Right) Total pressure fluctuations

Figure 5 – Vertical distributions of dimensionless time-averaged total pressure and total pressure fluctuations in the turbulent shear region – Flow conditions: Q = 0.0347 m^3/s, d_1 = 0.020 m, x_1 = 0.83 m, Fr_1 = 7.5, Re = 6.8×10^4.

The total pressure measurements were only valid in the turbulent shear region where the interfacial velocity was positive. The results were presented relative to the atmospheric pressure. Some typical vertical distributions of dimensionless mean pressure $P/(0.5\times\rho\times V_1^2)$ and pressure fluctuations $p'/(0.5\times\rho\times V_1^2)$ are presented in Figures 5A and 5B respectively, at several longitudinal positions for Fr_1 = 7.5. In the shear region, the mean total pressure exhibited a maximum P_{max} at an elevation 0.5 <

y_{Pmax}/d_1 < 0.9, while the pressure fluctuation reached a maximum p'_{max} at en elevation within 1.2 < $y_{p'max}/d_1$ < 1.5. The maximum total pressure P_{max} decreased with increasing distance from the jump toe, reflecting the dissipation of kinetic energy and turbulence of the flow. The longitudinal decay of dimensionless maximum mean pressure $P_{max}/(0.5\times\rho\times V_1^2)$ was nearly identical for all flow conditions. On the other hand, the dimensionless maximum pressure fluctuations $p'_{max}/(0.5\times\rho\times V_1^2)$ were systematically higher at large Froude numbers.

The total pressure consisted of the piezometric pressure related to the depth and the kinetic pressure related to the velocity. In the bubbly flow region, the total pressure can be derived from the air-water flow properties:

$$P = \frac{1}{2}\times\rho_w\times(1-C)\times V^2 + \int_{y}^{y_{90}}\rho_w\times(1-C)\times dz \qquad (8)$$

where C and V are the time-averaged void fraction and interfacial velocity measurements respectively, ρ_w is the water density and y_{90} is a characteristic elevation where the void fraction equals 90%. The total pressure data were compared with the calculations based upon Equation (8). Some typical comparison is presented in Figure 6A at one cross section in the shear region for Fr_1 = 7.5. Some reasonable agreement was achieved between the two methods in the high-velocity region. Above this region, neither the air-water interfacial velocity nor total pressure measurements were accurate because of the presence of negative velocities.

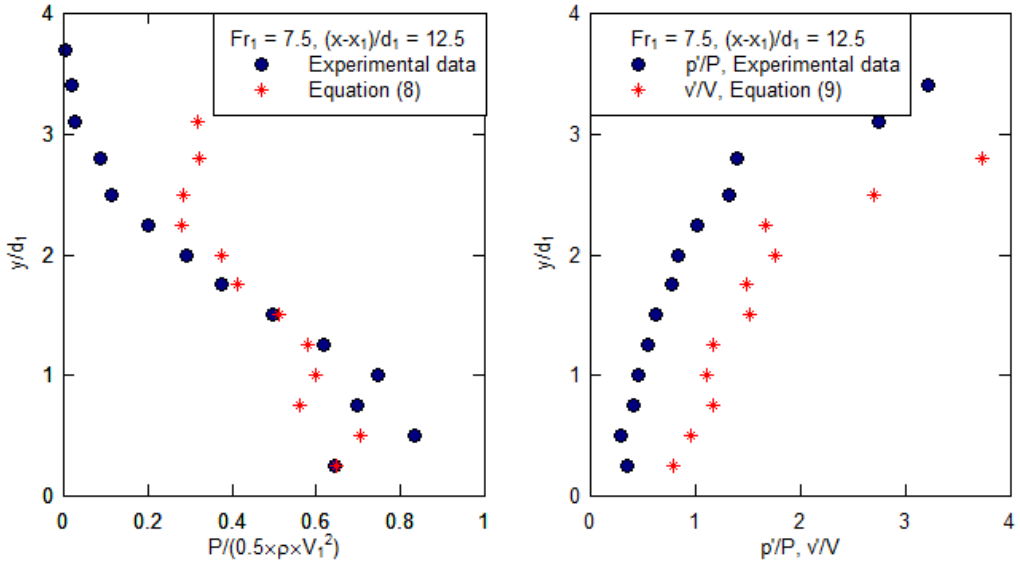

(A, Left) Vertical distributions of mean total pressure (B, Right) Vertical distribution of total pressure fluctuation and turbulence intensity

Figure 6 – Comparison between total pressure data and air-water flow measurements in the shear layer – Flow conditions: Q = 0.0347 m^3/s, d_1 = 0.020 m, x_1 = 0.83 m, $x-x_1$ = 0.25 m, Fr_1 = 7.5, Re = 6.8×10^4.

The relative total pressure fluctuation to local mean pressure p'/P was compared with the turbulence intensity v'/V derived from the air-water flow measurements. Correlation analyses of phase-detection probe sensor outputs gave an estimate of turbulence intensity (Chanson and Toombes 2002):

$$\frac{v'}{V} = 0.851\times\frac{\sqrt{\tau_{0.5}^2 - T_{0.5}^2}}{T} \qquad (9)$$

where v' is the longitudinal velocity fluctuation, T is the average time taken by a bubble travelling from the leading probe tip to the trailing tip, and $\tau_{0.5}$ and $T_{0.5}$ are some characteristic lag times shown in the correlation functions of the signals. Figure 6B shows a typical result for the same flow conditions as in

Figure 6A. Both p'/P and v'/V presented a monotonic increase with increasing distance from the bottom within the shear region. Although the turbulence intensity v'/V was consistently larger than the relative pressure fluctuation p'/P, the data exhibited a similar trend emphasising the strong link between the variations in total pressure and turbulent velocity. It is believed that the large turbulence intensities in the upper shear region (e.g. $2 < y/d_1 < 3.5$ in Fig. 6B) were related to the macroscopic variations in velocity field where the instantaneous flow reversal took place.

5. DISCUSSION: INSTANTANEOUS FLOW PROPERTY FLUCTUATIONS

Some correlation analyses were developed based upon the simultaneous measurements of instantaneous total pressure, void fraction and local water depth, thus providing some information on the co-variation of corresponding flow properties. Herein the correlation calculations involving the free surface data were performed on filtered signals below 50 Hz because of the relatively slow response of the acoustic displacement meters. For the pressure and phase-detection probe signals, the correlation calculations were conducted on filtered signals below 2 kHz.

Key parameters included the maximum/minimum correlation coefficients R_{max}. Figure 7 shows a typical sets of maximum correlation coefficients at the corresponding elevations, namely $(R_{yc})_{max}$ between the free surface fluctuations and instantaneous void fraction, $(R_{yp})_{max}$ between the free surface fluctuations and instantaneous total pressure and $(R_{pc})_{max}$ between the instantaneous total pressure and void fraction. The vertical distributions of the maximum correlation coefficients shown in Figure 7 were representative for all flows at most cross sections in the bubbly flow. The time-averaged void fraction profile is also plotted for completeness. In Figure 7, the coupling between instantaneous water elevation η and instantaneous void fraction c exhibited some negative correlation coefficients in the recirculation region ($y/d_1 > 3.3$), indicating synchronous increase in water level and decrease in void fraction. This may be understood considering the relative positions of the free surface and phase-detection probe tip. When the free surface fluctuations led to an increasing water depth, the air-water flow was measured at a deeper relative position from the free surface where the void fraction was lower. In the turbulent shear layer ($0 < y/d_1 < 3.3$), some positive correlations were shown in terms of both $(R_{yc})_{max}$ and $(R_{yp})_{max}$. The trends corresponded to simultaneous increase of instantaneous water level, void fraction and total pressure. The increasing water depth was the result of flow bulking caused by the entrainment of a large amount of air at the jump toe and their downstream advection in the shear layer. The total pressure fluctuation was associated with the change of piezometric pressure that was predominantly controlled by the free surface fluctuation.

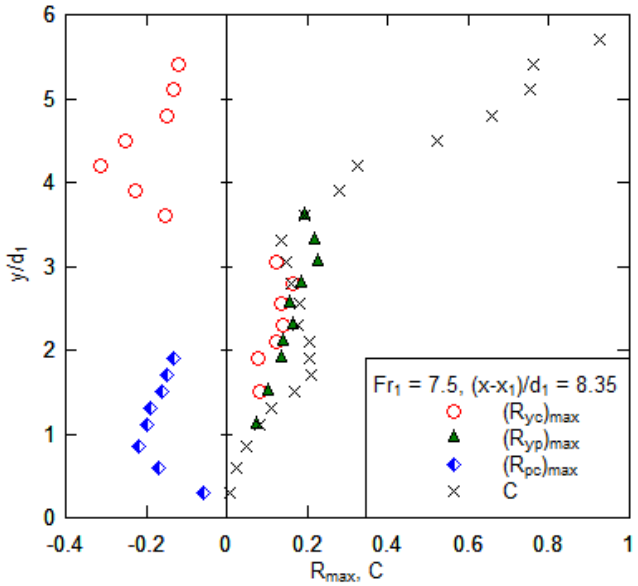

Figure 7 – Maximum correlation coefficients between the free surface fluctuations, instantaneous void fraction and total pressure – Flow conditions: Q = 0.0347 m^3/s, d_1 = 0.020 m, x_1 = 0.83 m, $x-x_1$ = 0.167 m, Fr_1 = 7.5, Re = 6.8×10^4.

The instantaneous total pressure and void fraction data were correlated with a much smaller time scale, thus reflecting the microscopic air-water flow processes. The negative correlations indicated a decreasing total pressure during an increasing void fraction, which might correspond to the arrival of one or a group of air bubble(s). This trend was mostly observed in a lower flow region with lesser aeration. It is emphasised that the time scale was different for the third correlation function (R_{pc}) compared to that for the other two correlation functions (R_{yc} & R_{yp}). The free surface fluctuations were coupled with the macro-scale air entrainment process and pressure variations, whereas the detection of air bubbles was coupled with the fast pressure fluctuations at a micro scale.

6. CONCLUSION

Detailed measurements were performed in hydraulic jumps with marked roller and substantial air entrainment. The total pressure field in a hydraulic jump was measured with a miniature probe. The local air-water flow properties and free surface positions were recorded simultaneously with the total pressure for Froude numbers from 3.8 to 8.5 and Reynolds numbers between 3.5×10^4 and 8×10^4. The free surface profiles presented some self-similarity within the roller length, while the free-surface fluctuation levels increased with increasing Froude numbers, showing a marked maximum in the first third of the roller. The distributions of time-averaged void fraction and air-water interfacial velocity were recorded in the entire jump roller area, and the two-phase flow data were used to validate successfully the total pressure measurements in the bubbly flow region. The time-averaged total pressure data presented some maximum at some elevation lower than the inflow depth. The maximum total pressure fluctuation was shown at some slightly higher elevation. Both maximum mean pressure and pressure fluctuations decreased in the streamwise direction. The comparison between dimensionless pressure fluctuation p'/P and turbulence intensity v'/V showed a similar trend.

The correlation analyses between simultaneous measurements of instantaneous total pressure, void fraction and local water depth provided some detailed information on the co-variation of corresponding two-phase flow parameters. The results revealed the contribution of piezometric pressure fluctuations to the total pressure fluctuations. Further correlations involving the instantaneous void fraction depicted the synchronous air entrainment in the turbulent shear region, flow bulking at the free surface and increase in total pressure at the macro scale. At a micro scale (millimetric and sub-millimetric), the presence of air bubbles was shown to be coupled with a drop in local total pressure. Altogether the findings demonstrated the complex interactions between the surface deformation, internal turbulence development and air entrainment in hydraulic jumps.

7. ACKNOWLEDGMENTS

The authors thank the technical staff of the School of Civil Engineering at the University of Queensland for their assistance. The financial support of the Australian Research Council (Grant DP120100481) is acknowledged.

8. REFERENCES

Avery, S.T., and Novak, P. (1978), *Oxygen Transfer at Hydraulic Structures*, Journal of Hydraulic Division, ASCE, Vol. 104, No. HY11, pp. 1521-1540

Chanson, H. (1995), *Air Entrainment in Two-dimensional Turbulent Shear Flows with Partially Developed Inflow Conditions*, International Journal of Multiphase Flow, Vol. 21, No. 6, pp. 1107-1121

Chanson, H. (2009), *Current Knowledge in Hydraulic Jumps and Related Phenomena. A Survey of Experimental Results*, European Journal of Mechanics B/Fluids, Vol. 28, No. 2, pp. 191-210 (DOI: 10.1016/j.euromechflu.2008.06.004)

Chanson, H. (2010). *Convective Transport of Air Bubbles in Strong Hydraulic Jumps*. International Journal of Multiphase Flow, Vol. 36, No. 10, pp. 798-814 (DOI: 10.1016/j.ijmultiphaseflow.2010.05.006)

Chanson, H. (2012), *Momentum Considerations in Hydraulic Jumps and Bores*, Journal of Irrigation and Drainage Engineering, ASCE, Vol. 138, No. 4, pp. 382-385 (DOI: 10.1061/(ASCE)IR.1943-4774.0000409)

Chanson, H. (2013), *Hydraulics of Aerated Flows: Qui Pro Quo?* Journal of Hydraulic Research, IAHR, Invited Vision paper, Vol. 51, No. 3, pp. 223-243 (DOI: 10.1080/00221686.2013.795917)

Chanson, H., and Toombes, L. (2002), *Air-Water Flows down Stepped Chutes: Turbulence and Flow Structure Observations*, International Journal of Multiphase Flow, Vol. 28, No. 11, pp. 1737-1761 (ISSN 0301-9322)

Hager, W.H. (1992), *Energy Dissipators and Hydraulic Jump*. Kluwer Academic Publ., Water Science and Technology Library, Vol. 8, Dordrecht, The Netherlands, 288 pages

Kucukali, S., and Chanson, H. (2007), *Turbulence in Hydraulic Jumps: Experimental Measurements*. Research Report No. CH62/07, Dept. of Civil Engineering, The University of Queensland, Brisbane, Australia, 40 pages (ISBN 9781864998825)

Liggett, J.A. (1994), *Fluid Mechanics*, McGraw-Hill, New York, USA

Murzyn, F., Mouaze, D., and Chaplin, J.R. (2007), *Air-water Interface Dynamic and Free Surface Features in Hydraulic Jumps*, Journal of Hydraulic Research, IAHR, Vol. 45, No. 5, pp. 679-685 (DOI: 10.1080/00221686.2007.9521804)

Murzyn, F., and Chanson, H. (2008), *Experimental Assessment of Scale Effects Affecting Two-Phase Flow Properties in Hydraulic Jumps*, Experiments in Fluids, Vol. 45, No. 3, pp. 513-521 (DOI: 10.1007/s00348-008-0494-4)

Murzyn, F., and Chanson, H. (2009), *Experimental Investigation of Bubbly Flow and Turbulence in Hydraulic Jumps*, Environmental Fluid Mechanics, Vol. 9, No. 2, pp. 143-159 (DOI 10.1007/s10652-008-9077-4)

Roache, P.J. (2009), *Perspective: Validation – What Does It Mean?* Journal of Fluids Engineering, ASME, Vol. 131, Paper 034503, (DOI: 10.1115/1.3077134)

Wang, H., and Chanson, H. (2013), *Free-Surface Deformation and Two-Phase Flow Measurements in Hydraulic Jumps*. Research Report No. CH91/13, School of civil Engineering, The University of Queensland, Brisbane, Australia, 108 pages (ISBN 9781742720746)